Received: 21 June 2019 | Revised: 3 December 2019 | Accepted: 3 January 2020

DOI: 10.1002/nag.3048

RESEARCH ARTICLE

WILEY

A semianalytic time-resolved poro-elasto-plastic model for wellbore stability and stimulation

Peter A. Fokker[1,2] | **Aditya Singh**[1] | **Brecht B.T. Wassing**[2]

[1]HPT Lab, Utrecht University, Utrecht, The Netherlands

[2]TNO Applied Geoscience, Utrecht, The Netherlands

Correspondence
Peter A. Fokker, HPT Lab, Utrecht University, Utrecht, The Netherlands.
Email: peter.fokker@tno.nl

Funding information
European Union, Grant/Award Numbers: 691728, 727550

Summary

Wellbore stability problems and stimulation operations call for models helping in understanding the subsurface behaviour and optimizing engineering performance. We present a fast, iteratively coupled model for the flow and mechanical behaviour that employs a time-sequential approach. Updates of pore pressure are calculated in a timestepping approach and propagated analytically to updates of the mechanical response. This way, the spatial and temporal evolution of pressure and mechanical response around a wellbore can be evaluated. The sequential approach facilitates the incorporation of pressure diffusion and of time-dependent plasticity. Also, it facilitates the implementation of permeability evolving with time, due to plasticity or stimulation. The model has been validated by means of a coupled numerical simulator. Its capabilities are demonstrated with a selection of sensitivity runs for typical parameters. Ongoing investigations target geothermal energy operations through the incorporation of thermo-elastic stresses and more advanced plasticity models.

KEYWORDS

coupled modelling, geothermal systems, stimulation, wellbore stability

1 | INTRODUCTION

The worldwide application of subsurface operations like the exploitation of geothermal energy is increasing and is expected to continue to increase dramatically in the near future. Along with this broader application, target areas are becoming increasingly more complicated. An example of this development is that geothermal operations and shale gas are increasingly often deployed in low-permeability reservoir rocks, which require stimulation for economic operations.[1,2] Another example is their deployment in sensitive areas, like tectonically active regions, which increases the risk of seismicity.[3] Also, the application will partly shift to depths where classical constitutive models do not apply and new ones must be developed.[4] Such characteristics all call for continued modelling investments. The geothermal industry being specifically targeting hot rocks with a crucial role for the mechanical response, such modelling, must couple flow with thermal and mechanical behaviour, let alone the chemical issues of scaling, precipitation, solution, acid reactions, and others.

Understanding the subsurface response to operations is not a goal in itself. Modelling needs to be connected to economics and safety. Now, economic and safety performance drivers are connected to modelling in several ways. Firstly,

engineering needs to be able to make faithful forecasts. Then, such forecasts can be used in an optimization schedule to support decision making. Fact-based decision making is required in many circumstances—some examples being the warranting of wellbore stability, the design of reservoir stimulation, and the minimization of induced seismicity.[5,6]

Quality decisions must be based on quality knowledge. Crucial in such knowledge is its quantified reliability, or uncertainty. When uncertainty ranges are not implicit part of the models, such quantification can be achieved by mapping the effect of uncertainty ranges of parameters to the forecast outcomes through the running of many model realizations.[7] A common approach to this is by doing parametric studies. In other cases, when data are available, data assimilation or history matching can be employed to improve the understanding and forecasting. Such applications, as well as the optimization of operational decisions, are often performed with stochastic methods as ensemble Kalman filters[8] and Monte Carlo, implying the execution of a forward model many times with parameters chosen from confidence ranges or operational ranges. Other methods, like grid searches, genetic algorithms, gradient searches, and particle filters, also require many runs of a forward model. For induced seismicity, the argument is even stronger because seismicity forecasts themselves have a stochastic character .[9]

These arguments do not imply that CPU-intensive, comprehensive models are not important. They have their use in deeply understanding the peculiar response of complex geological realizations, complex reservoirs, and complex well configurations. However, there is also a need for fast models with enough complexity to catch the essentials of the coupled subsurface behaviour that are still applicable in data assimilation and optimization, to yield quantified reliability. The realization of such an iteratively coupled model is the subject of the present investigation.

An extensive body of literature can be found on fast coupled subsurface models—many of them dating back a considerable amount of time, when numerical models were not yet ubiquitously available. Far from attempting to be comprehensive, we provide some highlights. Bai and Abousleiman[10] provided a useful overview of when certain couplings are required and when they can be ignored. Generally speaking, analytic or semianalytic coupled models have their merit in developing understanding of important features of the couplings investigated. For instance, fully transient analytical coupled models provide insight in the temporal development of stresses and pressures upon injection or production in a linear poro-elastic medium.[11] A clear outcome is the pressure diffusivity constant being different from the value in an uncoupled model, which is due to the pore compressibility.[12] Another insight from these authors is that under some circumstances, failure can initiate inside the rock rather than at the wellbore. A further example is given by Bai and Roegiers,[13] who showed that coupling of mechanics, temperature, and flow in a double-porosity medium may induce unexpected behaviour like a pressure rebound. Tao and Ghassemi[14] showed how effects due to coupling can play a role in engineering decisions. They specifically mentioned strength effects due to temperature variations. The fast models that fundamentally account for time-dependent behaviour, however, generally do not incorporate non-elastic behaviour like failure or plasticity.

Other models do incorporate failure and plastic behaviour. Wang and Dusseault[15] targeted hydraulic fracture initiation. They calculated stresses around the wellbore according to plasticity and showed that breakdown pressures cannot be determined based on an elastic treatment. The pore pressure was incorporated as a steady-state contribution. With a similar approach, Han and Dusseault[16] assessed changes in porosity and permeability based on elastic—perfectly plastic behaviour. They also used steady-state pressure distributions. Masoudian and Hashemi[17] built upon this approach by incorporating absorption-induced mechanics and permeability changes. In a follow-up paper,[18] targeting fractured reservoir, they noted the importance of incremental models that catch the time dependence. Most of these approaches address plasticity with an elastic—perfectly plastic scheme or an elastic—brittle—perfectly plastic scheme. Researchers having worked on more advanced constitutive models usually consider less coupling. An example is the work by Chen and Abouleiman, who worked on the modified Cam-clay model[19] and on the Drucker-Prager criterion-based strain hardening and strain softening model.[20]

Fundamental problems remain when applying these models to the problems sketched above. The transient models do not incorporate plasticity. The plasticity models on the other hand are not rigorously transient. They do not incorporate continued plastic flow. They take the pressure field as static and base their treatment on a steady-state situation. This is not realistic, as injection or production induces changing pressures and associated stresses. Neither of the two model classes can assess incremental plasticity, changing permeabilities, variable injection and production rates, well shut-in, or flowback. An engineering tool must incorporate such features in order to be applicable to realistic scenarios.

In this work, we undertake to fill these gaps. We present a semianalytical model in which the time-dependent behaviour is treated with an incremental setup. It mimics iteratively coupled numerical models in the sense that output of mechanical and of hydraulic calculations are mutual input in a time-sequential manner.[21,22] Plastic behaviour is one of its fundamental ingredients, along with the time-dependent pressure development. The setup enables to address all

the issues listed above, including stimulation and progressive failure. Current limitations include the radial symmetry, a plane-strain stress solution, isothermal operations, and an elastic-perfectly plastic constitutive model. We are addressing the issues of thermal effects and of more advanced plastic models in ongoing research and intend to report on the results in the near future. These issues are crucial for geothermal operations.

In the following sections, we will first lay out the model fundamentals. Then we will show some of the possibilities for representative cases and present a validation using a coupled numerical tool. Before we close the paper with conclusions, we provide a discussion of the model's potential and limitations, and an outlook to future work.

2 | MODELLING APPROACH

We are interested primarily in the transient behaviour of wells completed over a considerable interval. Therefore, we formulate our treatment for radial symmetry and for plane-strain conditions. We will treat the rock as a single-porosity medium with effective properties characterizing its behaviour. Some of the presumptions may be extended later.

Before the start of injection or production operations, a distortion of the in situ stress field already exists due to the presence of the well and the inner boundary conditions on it. Indeed, the radial stress in the formation at the well radius of an open hole must equal the internal fluid pressure. The elastic solution that is available for this situation may not be appropriate, however, failure can occur in the formation around the well when a failure criterion is exceeded. We employ a Mohr-Coulomb criterion, which presumes failure once the shear stress on a plane exceeds a linearly increasing function of the normal stress in the same plane. Under the assumption that the most critical stress in the plastic zone is at the Mohr-Coulomb failure envelope, the radial distribution of horizontal stresses can be calculated. In the elastic region, they follow linear elasticity. The plasticity radius is calculated based on the requirements of continuity of the horizontal radial stress at it and of the advance of the failure envelope at its elastic side. For the strains and displacements, Hooke's law is applied in the elastic zone; in the plastic zone, a perfectly plastic flow rule is employed. The radial displacement must be continuous at the plastic-elastic interface—this constrains the integration constant present in the solution to the flow rule.

After the start of pumping, be it production or injection, the pressure field around the well changes. The effect of this change on the mechanical behaviour can be described using linear poro-elasticity if it falls in the elastic regime. Whether or not this is the case must be determined by adding the stress increment calculated with poro-elasticity to the actual stress and applying the failure criterion to the result. If failure is indicated, additional plasticity is incorporated. All contributions are additions to the existing fields, which makes the treatment truly incremental.

The pore pressure is a key ingredient in the determination of the stress field. However, the pressure field development is coupled with the mechanical development. We follow the description of linear poro-elasticity[11,12,14] to formulate the full transient diffusivity equation—it deploys a diffusivity constant different from the traditional one in which flow only is considered: the effect of the poromechanical response is incorporated. The diffusivity equation can be solved under the assumption that the boundary conditions are known and the parameters are constant. However, the parameters prevalent in the diffusivity equation are not constant. Therefore, we employ a semisteady-state solution similar to the one by Dake[23] and by Grant and Bixley.[24] We use the value of the coupled diffusivity to estimate the radius up to which the pressure is disturbed; within this radius, we calculate the pressure using fully developed flow equations. This enables easy incorporation of time-dependent and position-dependent values for the mobility as well as changing rates. Mobilities are changed according to the output of the mechanical calculations.

2.1 | The linear poro-elastic regime

Linear elasticity involves a linear relationship between stress and strain. Poro-elasticity extends that by a linear effect of pore pressure on the stress—or, conversely, on the strain. When formulated as an effect on the stress, the additional terms are an additional isotropic stress term proportional to the changes in pore pressure. The proportionality is Biot's effective stress coefficient ($\alpha = 1 - \frac{K}{K_s}$; with K and K_s the rock's bulk modulus and the bulk modulus of the solid grains ($K = \frac{E}{3(1-2\nu)} = \frac{2G(1+\nu)}{3(1-2\nu)}$; E is the Young's modulus; G is the shear modulus; and ν is the Poisson ratio). We thus obtain

(with the sign convention that compressive normal stresses and strains be negative) the following relationships between induced total stress σ_{ij}, strain ε_{ij}, and pore pressure increase ΔP[12]

$$\sigma_{ij} = 2G\left[\varepsilon_{ij} + \frac{\nu}{1-2\nu}\varepsilon\delta_{ij}\right] - \alpha\Delta P\delta_{ij} + \sigma_{ij}^{\infty}. \tag{1}$$

These stresses include the fields already existing without pressure and temperature disturbance, σ_{ij}^{∞}; the strains are with respect to the strains in those background fields.

We assume that the system is in plane strain and has axial symmetry, and we change to axial coordinates with only radial displacements (u_r), and principal strains and stresses in radial, tangential, and vertical directions (ε_{rr},σ_{rr},$\varepsilon_{\theta\theta}$,$\sigma_{\theta\theta}$,$\varepsilon_{zz}$,and σ_{zz}). The vertical strain then vanishes ($\varepsilon_{zz} = 0$); the horizontal strains depend on the radial displacement only ($\varepsilon_{rr} = \frac{\partial u_r}{\partial r}; \varepsilon_{\theta\theta} = \frac{u_r}{r}$). Stress equilibrium in the horizontal plane is given in polar coordinates as $\frac{\partial\sigma_{rr}}{\partial r} + \frac{\sigma_{rr}-\sigma_{\theta\theta}}{r} = 0$. Substitution yields a differential equation for the radial displacement that can be solved to

$$u_r(r,t) = \frac{1}{r\cdot 2G}\left\{ I_{\mathrm{PT}}(r,t) + Z_1 + \frac{1}{2}Z_2 r^2 \right\},$$

$$I_{PT}(r,t) = \frac{1-2\nu}{1-\nu}\cdot\int_{r_w}^{r} \rho\cdot\alpha\Delta P(\rho,t)d\rho. \tag{2}$$

The difference of this expression as compared with the one usually given[12] is that we retain the second integration constant Z_2. The background of this choice is that we have not yet set the boundary conditions; we will show later that it is possible to have elastic regions that are bounded at an upper radius by a plastic region. We do, however, retain the most outer boundary at infinity. Further, the lower integral bound r_w is chosen freely, which is allowed because the integral constants can still be chosen freely.

Our treatment is intended to be incremental. Therefore, we need to calculate displacements, strains and stresses incremental to an existing field. We consider a time increment from t^i to t^{i+1} at the start of which we have displacement, strains, and stresses u_r^i, ε^i, and σ^i, and we write the fields at time t^{i+1} as the field at t^i plus an increment due to the update of the pressure field. With the definition of strain given above and the expression for the stresses in Equation (1), we calculate

$$\begin{aligned}
u_r^{i+1} &= u_r^i + \frac{1}{r\cdot 2G}\left\{ \Delta I_{PT}^{i+1} + Z_1^{i+1} + \frac{1}{2}Z_2^{i+1}r^2 \right\} && (a)\\
\varepsilon_{rr}^{i+1} &= \varepsilon_{rr}^i + \frac{1}{2G}\cdot\frac{1-2\nu}{1-\nu}\cdot\alpha\Delta P^{i+1} - \frac{1}{2Gr^2}\left\{ \Delta I_{PT}^{i+1} + Z_1^{i+1} - \frac{1}{2}Z_2^{i+1}r^2 \right\} && (b)\\
\varepsilon_{\theta\theta}^{i+1} &= \varepsilon_{\theta\theta}^i + \frac{1}{2Gr^2}\left\{ \Delta I_{PT}^{i+1} + Z_1^{i+1} + \frac{1}{2}Z_2^{i+1}r^2 \right\} && (c)\\
\varepsilon_{zz} &= 0 && (d)\\
\varepsilon^{i+1} &= \varepsilon_{rr}^{i+1} + \varepsilon_{\theta\theta}^{i+1} + \varepsilon_{zz}^{i+1} = \varepsilon^i + \frac{1}{2G}\cdot\frac{1-2\nu}{1-\nu}\cdot\alpha\Delta P^{i+1} + \frac{1}{2G}Z_2^{i+1} && (e)\\
\sigma_{rr}^{i+1} &= \sigma_{rr}^i - \frac{1}{r^2}\left[\Delta I_{PT}^{i+1}(r,t) + Z_1^{i+1}\right] + \frac{Z_2^{i+1}}{2(1-2\nu)} && (f)\\
\sigma_{\theta\theta}^{i+1} &= \sigma_{\theta\theta}^i - \frac{1-2\nu}{1-\nu}\cdot\alpha\Delta P^{i+1} + \frac{1}{r^2}\left[\Delta I_{PT}^{i+1}(r,t) + Z_1^{i+1}\right] + \frac{Z_2^{i+1}}{2(1-2\nu)} && (g)\\
\sigma_{zz}^{i+1} &= \sigma_{zz}^i - \frac{1-2\nu}{1-\nu}\cdot\alpha\Delta P^{i+1} + \frac{Z_2^{i+1}\nu}{1-2\nu} && (h)\\
\Delta I_{PT}^{i+1}(r,t) &= \frac{1-2\nu}{1-\nu}\cdot\int_{r_w}^{r}\rho\cdot\alpha\Delta P^{i+1}d\rho. && (i)
\end{aligned} \tag{3}$$

These expressions are independent of the precise form of the pressure distribution. Further, the total strain ε contains neither the integration constant Z_1 nor the integral $\Delta I_{PT}(r,t)$. The integration constants Z_1 and Z_2 must later be determined when the boundary conditions are applied. If the elastic regime extends to infinity, Z_2 is chosen 0 because displacements in infinity must vanish.

2.2 | Pressure field approximation

The transient pressure solution in an infinite homogeneous poro-elastic medium can be found by writing down the water content variation with strain and pressure, coupling this with the Darcy flow equation and substituting for the total strain the expression given in the previous Section.[11,12] A linear diffusivity equation then is obtained with modified diffusivity with respect to the diffusivity of flow that is not coupled to deformation:

$$\frac{\partial^2 P}{\partial r^2} + \frac{1}{r}\frac{\partial P}{\partial r} = c\frac{\partial P}{\partial t},$$

$$c = \frac{1}{\lambda}\left[\frac{1}{M} + \frac{\alpha^2}{2G}\cdot\frac{1-2\nu}{1-\nu}\right]. \tag{4}$$

In this expression, $\lambda = \frac{k}{\mu}$, the ratio of permeability and viscosity, is the mobility; M is a Biot modulus[47] defined as $M = \frac{\frac{K_f}{\phi}}{\left[1+\frac{K_f}{\phi K_s}\left(1-\phi-\frac{K}{K_s}\right)\right]}$ in which K_f, K_s, and K are the bulk moduli of the fluid, the solid grains and the rock, respectively; and ϕ is the porosity. For constant parameters, we have the general solution of the diffusivity equation, with a flow Q_{inj} starting at time $t = 0$:

$$P(r,t) = P_0 + \frac{\tilde{Q}}{4\lambda}E_1\left(\frac{cr^2}{4t}\right),$$

$$\tilde{Q} = \frac{Q_{\text{inj}}}{\pi h}, \tag{5}$$

in which the far-field pressure P_0 has been incorporated.

We were looking for a more flexible approach with parameters possibly variable in space and time. The permeability may have changed due to reservoir stimulation or plastic behaviour of the reservoir rock. Even in the region where linear poro-elastic behaviour applies, the mean stress can change, affecting the permeability through a change in porosity. In addition, we want to anticipate future developments in which we wish to incorporate thermal effects and more advanced constitutive models. Therefore, the diffusivity is not constant and the diffusion equation cannot be solved under the assumption of constant parameters. We need an alternative for the exponential integral E_1.

The alternative approach that we take consists of the approximation of fully developed flow: it is semisteady state. The approximation is related to the fact that for values of $\frac{cr^2}{4t} < 0.01$, the exponential integral (Equation (5)) can be approximated with a natural logarithm. For large enough times, an equivalent solution can be formulated as a logarithmic decay up to an influence radius—the pressure drop within that radius can thus be calculated using Darcy's law under the assumption of negligible storage [,[24] p.36]. An additional argument to use this approximation is that we are mainly interested in the changes of stress close to the injection well, where the pressure changes are most significant. The region where the deviation from the logarithmic approximation is most severe shows the smallest changes in pressure. For the calculation of the influence radius, we use the diffusivity of the virgin formation since the movement of the radius of the pressure disturbance is located in that region.

In the semisteady-state approximation, the pressure resulting from injection with rate Q_{inj} (positive for injection) starting at time 0 is fully described by Darcy's law, the virgin pressure P_0, zero compression of the fluid, and an influence radius growing with time according to the virgin diffusivity. We have

$$\frac{dp}{dr} = -\frac{q(r)}{\lambda} = \frac{-\tilde{Q}}{2\lambda r}\,(for\, r < r_e(t)),$$

$$P(r,t) = P_0 + \int_r^{r_e(t)} \frac{\tilde{Q} d\rho}{2\lambda(\rho)\rho} \, (for\, r < r_e(t)),$$

$$r_e(t) = \sqrt{\frac{2.25 \cdot t}{c} + r_w^2}. \tag{6}$$

The term r_w^2 has been introduced to prevent radii smaller than the wellbore radius in such a way that the area within the influence radius grows linearly with time.

The injection rate is often applied for a finite time; or, alternatively, changes in the rate occur. Like in usual well testing approaches, we employ superposition of solutions with different rates, eg, equal opposite rates with different starting times for complete cessation of injection. We only have to make sure that we use the actual mobility as a function of time and place. The superposition is incorrect for short times after a change of rate, when the reservoir close to the well needs time to equilibrate with the new rate and the pressure disturbance moves at a different velocity. We thus need to treat results for such short timescales with care and check whether the approximation was permitted.

The pressure at a certain time thus is a superposition of the contributions of all periods j with their own injection rates and radii of influence until that time:

$$\Delta P(r, t_n < t < t_{n+1}) = \sum_{j=1}^{n} \int_{\min\left(r, r_e^j(t)\right)}^{r_e^j(t)} \frac{\tilde{Q}_j - \tilde{Q}_{j-1}}{2\lambda(\rho)\rho} d\rho,$$

$$r_e^j(t) = \sqrt{2.25 \cdot \frac{t - t_{j-1}}{c} + r_w^2}. \tag{7}$$

This expression can be inserted in the integral of Equations (2) and (3). The diffusivity equation is thus not used for the pressure solution; it has only served to determine the radius of the pressure disturbance developing with time. For this goal, the formulation in an infinite homogeneous medium is sufficient.

2.3 | The plastic zone

We employ perfect plasticity with the Mohr-Coulomb failure criterion. It indicates that failure occurs once the shear stress exceeds a maximum that is linearly dependent on the effective normal stress. With a friction coefficient $\mu = \tan\phi$ and cohesion S_0, we have $|\tau| = S_0 - \mu\sigma'^{pl}$ (the minus sign originates from the engineering convention of negative compressive stresses). For the effective stress for plasticity, we use the Terzaghi definition, $\sigma_{ij}'^{pl} = \sigma_{ij} + P\delta_{ij}$. As long as plastic behaviour lasts, stresses stay at the failure line. Strains develop according to a non-associated plastic flow rule.

If the plane of failure is not predetermined, failure will occur when the Mohr circle touches the failure envelope. The condition can then be translated to a relationship between the maximum and minimum effective principal stresses, $\sigma_1'^{pl}$ and $\sigma_3'^{pl}$ [25,47] :

$$\sigma_1'^{pl} = -2S_0\left(\sqrt{1+\mu^2} + \mu\right) + \sigma_3'^{pl}\left(\sqrt{1+\mu^2} + \mu\right)^2,$$

$$\sigma_1'^{pl} = -2S_0\sqrt{\gamma} + \gamma\sigma_3'^{pl},$$

$$\gamma = \frac{1+\sin\phi}{1-\sin\phi}. \tag{8}$$

This equation can be used to judge whether failure occurs. The elastic solution can be employed at locations where $\sigma_1'^{pl} > -2S_0\sqrt{\gamma} + \gamma\sigma_3'^{pl}$.

Perfect plasticity implies that the effective stress is at the failure line.[16] We thus combine Equation (8) with the equilibrium equation, in terms of effective horizontal stresses and with the pressure gradient given in Equation (6). In case

the tangential effective stress is the largest, $\sigma_{rr} = \sigma_3$; in the converse case, the radial effective stress is the largest: $\sigma_{rr} = \sigma_1$. For the two cases we thus have

$$\begin{cases} \sigma'^{pl}_{\theta\theta} = -2S_0\sqrt{\gamma} + \gamma\sigma'^{pl}_{rr} & (\sigma_{rr} = \sigma_3) \\ \sigma'^{pl}_{rr} = -2S_0\sqrt{\gamma} + \gamma\sigma'^{pl}_{\theta\theta} & (\sigma_{rr} = \sigma_1) \end{cases}.$$

This can be rephrased with a single equation but separate definition of γ and g_0:

$$\sigma'^{pl}_{\theta\theta} = \gamma\sigma'^{pl}_{rr} - g_0(\gamma),$$

$$\begin{cases} \gamma = \dfrac{1+\sin\phi}{1-\sin\phi} & g_0(\gamma) = 2S_0\sqrt{\gamma} \quad (\sigma_{rr} = \sigma_3) \\ \gamma = \dfrac{1-\sin\phi}{1+\sin\phi} & g_0(\gamma) = -2S_0\sqrt{\gamma} \quad (\sigma_{rr} = \sigma_1) \end{cases}. \tag{9}$$

The equilibrium equation can then be written as

$$\frac{d\sigma'_{rr}}{dr} - (\gamma - 1)\frac{\sigma'_{rr}}{r} = -\frac{1}{r}g(\gamma),$$

$$g(\gamma) = \frac{\tilde{Q}}{2\lambda} + g_0(\gamma). \tag{10}$$

Accounting for the inner boundary condition at r_A of $\sigma'_{rr}(r_A) = \sigma^A_{rr} + P^A$, this differential equation can be solved, giving horizontal plastic compressive effective and total stresses as

$$\begin{cases} \sigma'_{rr} = r^{\gamma-1}\left[\dfrac{\sigma^A_{rr} + P^A}{r_A^{\gamma-1}} - \displaystyle\int_{r_A}^{r} g(\rho)\rho^{-\gamma}d\rho\right], \\ \sigma'_{\theta\theta} = \gamma\sigma'_{rr} - g_0(\gamma) \end{cases}$$

$$\begin{cases} \sigma_{rr} = \sigma'_{rr} - P \\ \sigma_{\theta\theta} = \sigma'_{\theta\theta} - P \end{cases}. \tag{11}$$

If these equations need to be employed with the inner boundary at the wellbore, the inner boundary condition is a zero effective radial stress; $\sigma^A_{rr} = -P^A$ and the solution for σ'_{rr} simplifies to the integral only.

The strain in the study domain can have elastic and plastic components. This is also the case for the incremental strain resulting from the change in stress in a time increment from t^i to t^{i+1}. Following Masoudian et al[18], we write

$$\varepsilon^{i+1}_{jk} = \varepsilon^i_{jk} + \delta\varepsilon^{i+1}_{jk} = \varepsilon^i_{jk} + \delta\varepsilon^{e,i+1}_{jk} + \delta\varepsilon^{p,i+1}_{jk}. \tag{12}$$

We employ a nonassociated flow rule to find the displacement in the plastic zone. The radial and tangential components of the incremental plastic strain then are related through the dilation angle ψ as

$$\begin{cases} \delta\varepsilon^p_{rr} + \beta\delta\varepsilon^p_{\theta\theta} = 0 & (\sigma_{rr} = \sigma_3) \\ \beta\delta\varepsilon^p_{rr} + \delta\varepsilon^p_{\theta\theta} = 0 & (\sigma_{rr} = \sigma_1) \end{cases},$$

$$\beta = \frac{1+\sin\psi}{1-\sin\psi}.$$

This can be rephrased with a single equation but separate definition of β:

$$\delta\varepsilon_{rr}^{p} + \beta\delta\varepsilon_{\theta\theta}^{p} = 0,$$

$$\begin{cases} \beta = \dfrac{1+\sin\psi}{1-\sin\psi} & (\sigma_{rr} = \sigma_3) \\ \beta = \dfrac{1-\sin\psi}{1+\sin\psi} & (\sigma_{rr} = \sigma_1) \end{cases}. \tag{13}$$

Recalling the definition of strain, $\delta\varepsilon_{rr} = \frac{\partial\delta u_r}{\partial r}; \delta\varepsilon_{\theta\theta} = \frac{\delta u_r}{r}$ for radial symmetry, we can write a differential equation for the displacements δu as

$$\frac{\partial\delta u}{\partial r} + \beta\frac{\delta u}{r} = f(r), \tag{14}$$

in which the plastic deformation does not contribute to the function $f(r)$. It is fully determined by the elastic response to the stresses at work, ie, Hooke's law (Equation (1)). Like in the elastic case, the strains and displacement must be calculated with regard to the displacement at the previous timestep.

$$f(r) = \delta\varepsilon_{rr}^{e} + \beta\delta\varepsilon_{\theta\theta}^{e} = \frac{1}{2G(1+\nu)}\left\{(1-\beta\nu)\left(\sigma_{rr}-\sigma_{rr}^{i}\right) + (\beta-\nu)\left(\sigma_{\theta\theta}-\sigma_{\theta\theta}^{i}\right) - (1+\beta)\nu\left(\sigma_{zz}-\sigma_{zz}^{i}\right) + (1+\beta)(1-2\nu)\alpha\delta P\right\}. \tag{15}$$

Equation (14) can be solved with a numerical integration of the function $f(r)$. Formulating a boundary condition as a prescribed displacement at the inner boundary $\delta u(r_A) = \delta u_A$, we then obtain

$$u^{i+1}(r) = u^{i}(r) + \delta u_A\left(\frac{r}{r_A}\right)^{-\beta} + r^{-\beta}\int_{r_A}^{r}\rho^{\beta}f(\rho)d\rho,$$

$$\varepsilon_{rr}^{i+1} = \varepsilon_{rr}^{i} - \frac{\beta}{r}\left[\delta u_A\left(\frac{r}{r_A}\right)^{-\beta} + r^{-\beta}\int_{r_A}^{r}\rho^{\beta}f(\rho)d\rho\right] + f(r),$$

$$\varepsilon_{\theta\theta}^{i+1} = \varepsilon_{\theta\theta}^{i} + \frac{1}{r}\left[\delta u_A\left(\frac{r}{r_A}\right)^{-\beta} + r^{-\beta}\int_{r_A}^{r}\rho^{\beta}f(\rho)d\rho\right]. \tag{16}$$

2.4 | Incremental solution

We have now laid down the fundamental equations for the incremental solution that we were seeking. The following step is to connect the solutions in the different elastic and plastic zones. This is possible by fixing the integration constants using inner and outer boundary conditions, and interface conditions at the elastic-plastic transition radii.

We first address the starting solution for the total domain. This is straightforward and has also been done by other researchers, as the solution employs neither timestepping nor pressure disturbances.[16,17]

We first calculate the stresses according to the elastic solution from Equation (3) with vanishing pressure disturbance, vanishing integral I_{PT}^{1}; $Z_2^1 = 0$ because of vanishing fields at infinity, and an initial horizontal and vertical stress equal to the virgin values σ_h^{∞} and σ_z^{∞}:

$$\sigma_{rr}^{1} = \sigma_h^{\infty} - \frac{Z_1^1}{r^2},$$

$$\sigma_{\theta\theta}^{1} = \sigma_h^{\infty} + \frac{Z_1^1}{r^2},$$

$$\sigma_{zz}^{1} = \sigma_z^{\infty}. \tag{17}$$

If the solution applies to the complete domain, we have $Z_1^1 = r_w^2\left(P_w + \sigma_h^{\infty}\right)$ because of the inner boundary condition $\sigma_{rr}^1(r_w) = -P_w$. When the elastically calculated stress concentration at the wellbore is larger than allowed by the Mohr-Coulomb failure criterion, a plastic zone around the wellbore develops. Application of the condition at the wellbore to Equation (11) then gives $\sigma_{rr}^A = -P_w$. Further, we take $\sigma_3 = \sigma_{rr}$, ie, the wellbore pressure does not exceed the initial horizontal in-situ stress. Then, with no pressure disturbance in the reservoir ($P = P_w$), the plastic stresses can be calculated analytically:

$$\sigma_{rr} = 2S_0\sqrt{\gamma}\left\{\frac{1}{\gamma-1}\left[1-\left(\frac{r}{r_w}\right)^{\gamma-1}\right]\right\} - P_w,$$

$$\sigma_{\theta\theta} = 2S_0\sqrt{\gamma}\left\{-1+\frac{\gamma}{\gamma-1}\left[1-\left(\frac{r}{r_w}\right)^{\gamma-1}\right]\right\} - P_w. \tag{18}$$

At the plasticity radius r_p, the radial stress must be continuous. At the elastic side of the radius, the stresses must be critical according to the failure line—for the current implementation with elastic-perfectly plastic material this implies continuity of the tangential stress as well. We obtain

$$\sigma_h^{\infty} - \frac{Z_1^1}{r_p^2} = 2S_0\sqrt{\gamma}\left\{\frac{1}{\gamma-1}\left[1-\left(\frac{r_p}{r_w}\right)^{\gamma-1}\right]\right\} - P_w,$$

$$\sigma_h^{\infty} + \frac{Z_1^1}{r_p^2} = 2S_0\sqrt{\gamma}\left\{-1+\frac{\gamma}{\gamma-1}\left[1-\left(\frac{r_p}{r_w}\right)^{\gamma-1}\right]\right\} - P_w, \tag{19}$$

The term $\frac{Z_1^1}{r_p^2}$ can be eliminated, and we obtain analytic expressions for r_p and Z_1^1

$$r_p = r_w\left\{1-\frac{2\sigma_h^{\infty}+2P_w+2S_0\sqrt{\gamma}}{2S_0\sqrt{\gamma}}\cdot\frac{\gamma-1}{\gamma+1}\right\}^{\frac{1}{\gamma-1}},$$

$$\frac{Z_1^1}{r_p^2} = \sigma_h^{\infty} + P_w - \frac{1}{\gamma+1}\cdot\left\{2\sigma_h^{\infty}+2P_w+2S_0\sqrt{\gamma}\right\}. \tag{20}$$

Finally, continuity of displacement gives

$$u_A = \left(\frac{r_p}{r_w}\right)^{\beta}\left\{\frac{Z_1^1}{r_p\cdot 2G} - r_p^{-\beta}\int_{r_w}^{r_p}\rho^{\beta}\left[f_1(\rho)\sigma_{rr}^A + f_2(\rho)\right]d\rho\right\} \tag{21}$$

In the last step, the function $f(\rho)$ in the integrand (cf. Equation (15)) has been written as

$$f(r) = f_1(r)\sigma_{rr}^A + f_2(r),$$

$$f_1(r) = \frac{1-\beta\nu+\beta\gamma-\gamma\nu}{2G(1+\nu)} \cdot \left(\frac{r}{r_A}\right)^{\gamma-1},$$

$$f_2(r) = -\frac{1-\beta\nu+\beta\gamma-\gamma\nu}{2G(1+\nu)}\left[\left(\frac{r}{r_A}\right)^{\gamma-1} P^A + r^{\gamma-1}\int_{r_A}^{r} g(\rho)\rho^{-\gamma}d\rho\right] \cdot \frac{1\text{-}\beta\nu+\beta\text{-}\nu}{2G(1+\nu)}P(r) - \frac{1-\beta\nu}{2G(1+\nu)}\sigma_{rr}^i - \frac{\beta-\nu}{2G(1+\nu)}\left(\sigma_{\theta\theta}^i \pm 2S\sqrt{\gamma}\right) \tag{22}$$
$$+ \frac{1+\beta}{2G(1+\nu)}\left[-\nu\left(\sigma_{zz}-\sigma_{zz}^i\right) + (1-2\nu)\alpha\delta P\right].$$

After starting the pumping, multiple elastic and plastic zones can evolve. For example, this can occur when an initially plastic—elastic complex evolves due to the increase of pore pressure: part of the plastic zone in the reservoir reacts plastically while close to the well the added stresses cause an elastic response on top of the already existing stress and displacement field. This was already noted by Detournay and Cheng[12] for the full transient solution with static properties.

Our approach is to incrementally change the pressure and mechanical fields at each timestep. Then the determination of the plasticity radius as outlined above for the first timestep is not necessary. We first calculate the supposedly elastic response on the incremental changes in pressure on the full domain. Then the regions in which the failure envelope is exceeded are determined using the resulting effective stresses. In those regions, the plastic response is calculated according to the assumption of stress on the failure line and the nonassociated flow rule, as detailed in Section 2.3. The integration constants at this point are not yet determined.

Because the plasticity radii are not free in this approach, we cannot force the stress at the elastic side of the elastic-plastic radii to be critical; we have to rely on the choice of the radius. We are, however, more flexible in the sense that more regions can be allowed. The mismatch is minimized by making small timesteps, and stability is guaranteed since a full new evaluation of criticality is performed in the next timestep.

We are thus starting from a stress profile at the previous timestep i, with stresses given by $\sigma_{rr}^i(r)$ and $\sigma_{\theta\theta}^i(r)$. Further, we have a pressure and temperature profile for the new timestep i+1 that results in an incremental integral given by $\Delta I_{PT}^{i+1}(r)$. We count the successive plastic and elastic regions with $l = 1..L$ and call the inner radius of a region r_{l-1} ($r_w = r_0$). Then, dropping the superscript for the time (i+1), we have as parameters for the elastic zones Z_{1l} and Z_{2l} for the elastic constants in Equation (3); for the plastic zones, we have $\sigma_{rr,l}^A$ and $\delta u_{A,l}$ for the radial stress and the displacement at the inner boundary of the plastic zone, from Equations (11) and (16). This way, we have 2L parameters.

The boundary and interface conditions that are used to determine the parameters give 2L equations:

1. Radial stress equals pressure in the wellbore (1 equation)
   If the inner zone is elastic:

$$\frac{Z_{1,1}}{r_w^2} - \frac{Z_{2,1}}{2(1-2\nu)} = \sigma_{rr}^i(r_w) + P_w. \tag{23}$$

   If the inner zone is plastic:

$$\sigma_{rr,1}^A = -P_w. \tag{24}$$

2. Continuity of radial stresses at interfaces between zone l and zone l+1, ie, at r_{l+1}; ($L-1$ equations)
   At elastic l to plastic l+1 interface

$$\sigma_{rr}^i(r_{l+1}) - \frac{1}{r_{l+1}^2}\left[\Delta I_{PT}^{i+1}(r_{l+1},t) + Z_{1,l}\right] + \frac{Z_{2,l}}{2(1-2\nu)} = \sigma_{rr,l+1}^A. \tag{25}$$

   At plastic l to elastic l+1 interface

$$\frac{r_{l+1}^{\gamma-1}}{r_l^{\gamma-1}}\sigma_{rr,l}^A + r_{l+1}^{\gamma-1}\left[\frac{P(r_l)}{r_l^{\gamma-1}} - \int_{r_l}^{r_{l+1}} g(\gamma)\frac{d\rho}{\rho^\gamma}\right] - P(r_{l+1}) = \sigma_{rr}^i(r_{l+1}) - \frac{1}{r_l^2}\left[\Delta I_{PT}^{i+1}(r_{l+1},t) + Z_{1,l+1}\right] + \frac{Z_{2,l+1}}{2(1-2\nu)}. \tag{26}$$

3. Continuity of displacements at interfaces ($L-1$ equations)
   At elastic l to plastic l+1 interface

$$\delta u_{A,l+1} = \frac{1}{r_{l+1}\cdot 2G}\left\{\Delta I_{PT}^{i+1}(r_{l+1}) + Z_{1,l} + \frac{1}{2}Z_{2,l}r_{l+1}^2\right\}. \tag{27}$$

   At plastic l to elastic l+1 interface

$$\delta u_{A,l}\left(\frac{r_{l+1}}{r_l}\right)^{-\beta} + \sigma_{rr}^A r_{l+1}^{-\beta}\int_{r_l}^{r_{l+1}}\rho^\beta f_1(\rho)d\rho + r_{l+1}^{-\beta}\int_{r_l}^{r_{l+1}}\rho^\beta f_2(\rho)d\rho = \frac{1}{r_{l+1}\cdot 2G}\left\{\Delta I_{PT}^{i+1}(r_{l+1}) + Z_{1,l+1} + \frac{1}{2}Z_{2,l+1}r_{l+1}^2\right\}. \tag{28}$$

4. No displacement at infinity (1 equation)

$$Z_{2L} = 0. \tag{29}$$

These equations are linear in the parameters and can thus be easily solved. For the convenience of the reader, a three-zone region (elastic-plastic-elastic) is detailed in Appendix A.

2.5 | Permeability modification

Finally, the loop must be closed with the effect of the mechanical response on injectivity. We can employ the total strain as input for porosity and permeability. The resulting permeability field can then be used as input for the pressure distribution at the subsequent timestep. We can also use a direct relationship between effective stress and permeability. The aperture of fractures in a fracture network is related to the permeability and changed when the porosity is changed due to changes in the mean effective stress. Within the sequential setup of our code, it is not difficult to implement different permeability models.

One of the interesting applications is in naturally fractured rocks. Therefore, we follow the line of thought of Bai and Elsworth[26] for fractured porous media. They assume that the effective permeability is fully determined by the fracture network and that opening of the fractures relates to the permeability through the cubic law. With a fracture spacing s and a fracture width b, the effective permeability is

$$k_{\text{eff}} = \frac{b^3}{12s}. \tag{30}$$

For a virgin formation with permeability k_0 and fracture spacing S, the initial fracture width $b_0 = \sqrt[3]{12k_0 s}$ can thus be calculated. This number does not have to relate directly to the porosity since there may be matrix porosity that is not contributing to flow. When a volumetric strain is present, this will affect the fracture width. Assigning the full strain to the opening of the fractures implies $b = b_0 + s\Delta\varepsilon$ with $\Delta\varepsilon$ the strain contribution to the fractures that facilitate flow in a certain direction. We do not take for $\Delta\varepsilon$ the strain perpendicular to the direction of flow, because there may also be contributions to flow through fractures under an angle—and taking the plane perpendicular to the fault plane in which the flow takes place could mean $\Delta\varepsilon = \varepsilon_{\theta\theta}$, which under normal circumstances is negative (compressive), while the radial component is positive. For the time being we take $\Delta\varepsilon = \frac{1}{2}(\varepsilon_{rr} + \varepsilon_{\theta\theta})$. The permeability will then be changed as

$$k = k_0\left(1+\frac{s\Delta\varepsilon}{b_0}\right)^3 = k_0\left(1+\frac{s\Delta\varepsilon}{\sqrt[3]{12k_0 s}}\right)^3 = k_0\left(1+\sqrt[3]{\frac{s^2}{12k_0}}\Delta\varepsilon\right).^3 \tag{31}$$

For the moment, we neglect the influence of shear strain on the permeability.

3 | EXAMPLE RESULTS AND VALIDATION

A basic first calibration run has been built for values typically pertinent to a Netherlands geothermal field with constant permeability: a 20 md reservoir of 30-m thickness at 2.5-km depth; 30 days injecting water at a rather low rate of 180 L/min. Reservoir properties and operational parameters are represented in Table 1.

Before starting injection we see in the stress output that a plastic zone is present with a diameter of 2.2 times the well radius (Figure 1). This results in the typical two-zone stress regime also observed by other authors (the purple curves in Figure 1). A plastic zone is present close to the well, both the radial and the tangential stresses in this region decrease monotonically up to a plasticity radius. At the plasticity radius, the gradient of the tangential stress switches sign; in the elastic region outside, the radial stress decreases further with larger radius, while the tangential stress increases until the two join in infinity at the virgin horizontal stress. The displacements are into the wellbore because the radial stress at the wellbore wall is decreased with respect to the virgin horizontal stress.

Upon the starting of injection, we see that the pressure disturbance enter the reservoir (Figure 1). Injection causes the wellbore pressure to increase; hence, we see a decrease of the radial stress. The tangential stress, however, is hardly affected. As a result, criticality of the system close to the wellbore is decreasing. Away from the wellbore and into the reservoir, plastic yielding continues inside the original plasticity radius. This is demonstrated with the plot with criticality vs radius. Displacements close to the wellbore are not affected much, but away from the wellbore, the movement becomes outward due to the pressurization, which is largest close to the well. Beyond the pressure influence, the displacements become smaller again; this behaviour falls outside the represented region for the larger times represented.

When a pressure falloff is added to the injection period, a number of observations can be made. In the first place, the pressure in the wellbore decreases. The influence of stopping injection gradually propagates into the reservoir; as a result a pressure plateau of decreasing value develops close to the well, with an increasing radius. We demonstrate this in Figure 2, where the development is represented at times past the moment of injection. The pressure development is accompanied by stress changes. Particularly, interesting are the criticality curves: while new plastic behaviour develops near the well, the zone is smaller than the originally yielded zone.

TABLE 1 Input parameters for the example runs and validation

Shared Parameters			
Depth, m	2500	E, GPa	15
H_{res}, m	100	K_{fluid}, GPa	2
R_w, m	0.1	ν, –	0.20
k, md	20	σ_h, MPa	−40
μ, mPa.s	0.365	α_{Biot}, –	1.0
ϕ, -	0.20	μ_{MC}, –	0.57
P_0, MPa	25	S_0, MPa	1.0
T, °C	80	ψ, –	0.10
Variable Parameters			
Case ID	Injection and Pressure Falloff	Stimulation and Pressure Falloff	Stimulation and Flowback
s_f, m	0	0.5	0.5
Q_{inj}, m^3/min	0.6-0.0	0.6-0.0	0.6 to −0.6
t_q, days	30-30	30-30	30-30

Note. The case labelled "stimulation" involves possible change of the permeability due *to fracture opening and closure.*

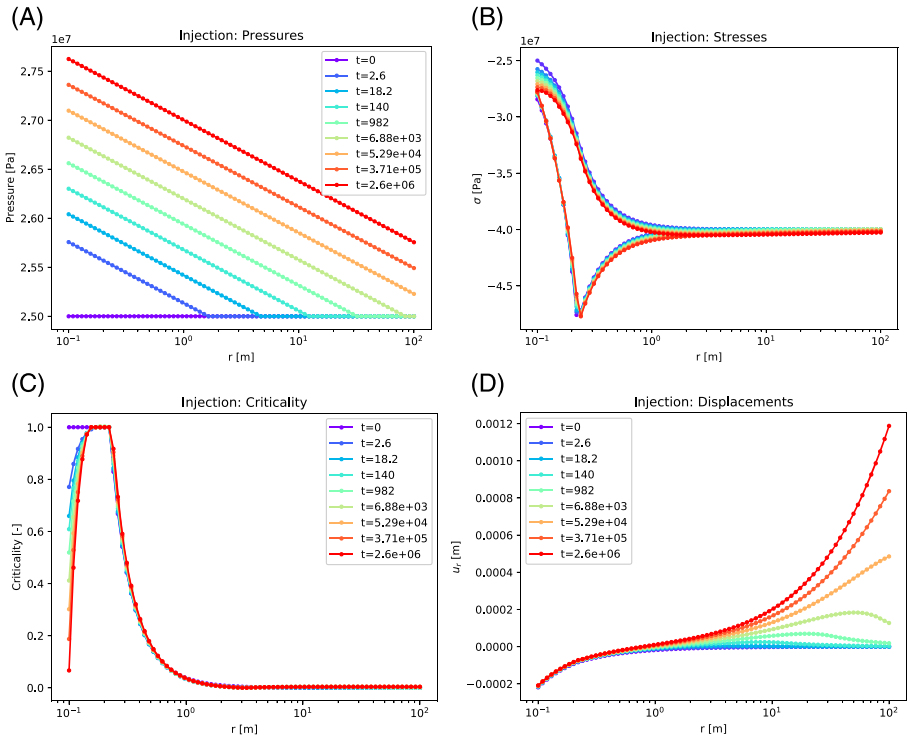

FIGURE 1 Fields for the injection case without permeability adaptation. The pressure disturbance moves into the reservoir with the development of time. The radial stresses (the upper ones) monotonically decrease towards infinity, the tangential ones decrease up to the initial plasticity radius and increase beyond it. Criticality at t=0 is 1 inside the plasticity radius; close to the wellbore is decreases upon the development of the pressure while away from the wellbore it remains 1. Displacements inside the reservoir develop due to the reservoir pressurization [Colour figure can be viewed at wileyonlinelibrary.com]

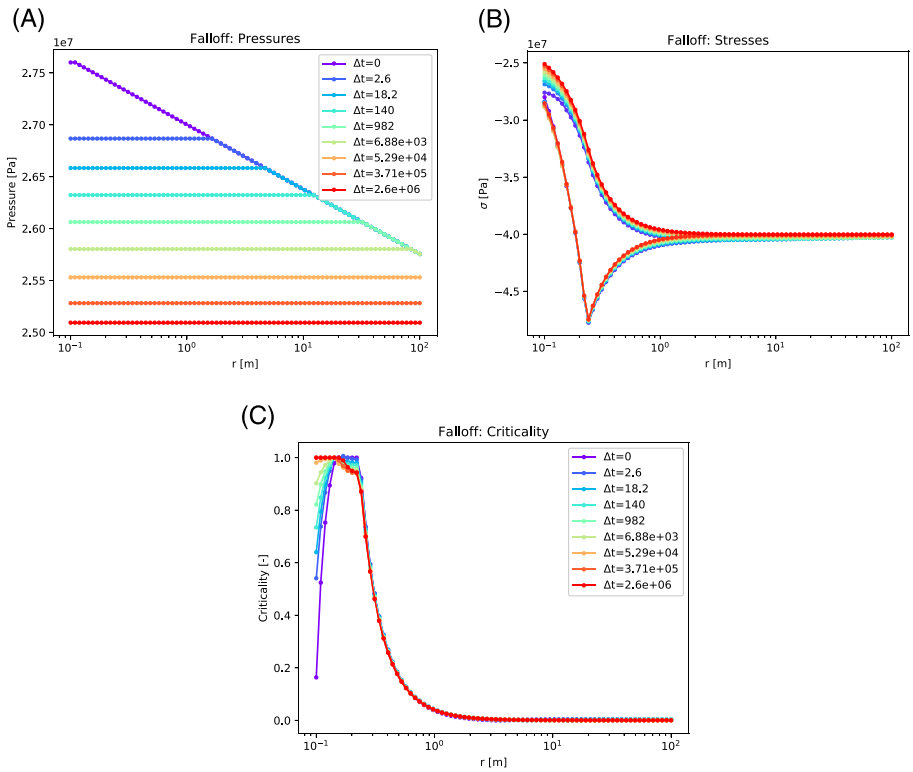

FIGURE 2 Fields for the injection-falloff case after shut-in. Pressures develop into a plateau of decreasing value with increasing radius. Stresses develop back towards the situation before pumping started, but not in the same way. Criticality during shut-in develops around the wellbore; further away the stress change is elastic [Colour figure can be viewed at wileyonlinelibrary.com]

A common way to display the stress development is to draft stress paths. Figure 3 shows the complete stress paths for a number of positions. Close to the wellbore, they start at the failure line but move away from it during injection, and back during shut-in. Further away, but still in the initial plastic regime, they move on the failure line during injection but slightly away from it during shut-in and pressure falloff. This is in accordance with the development of criticality as discussed in the previous paragraph. The previous plastic behaviour precludes reversibility. Beyond the plasticity radius, only the effective normal stresses react significantly, and virtually horizontal stress paths develop.

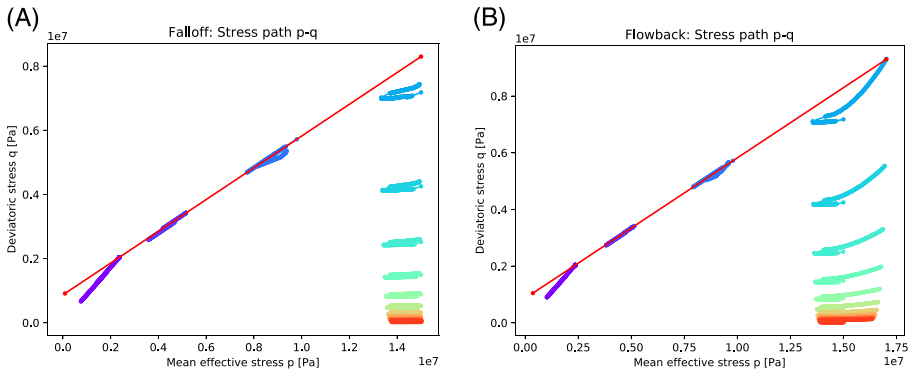

FIGURE 3 Stress paths at selected positions (each color representing a position—from blue to red at 0.108 m; 0.135 m, 0.179 m, and 0.213 m; and 0.268 m and further), for the complete injection-shut-in period. Stress paths are irreversible. Right figure: For injection-flowback. Stress paths start at the right and move left; at shut-in or flowback, they reverse their direction and move back right, further for the flowback (left picture). Colours ranging from blue to red indicate positions at increasing distance from the wellbore. The failure line is indicated with the red straight line [Colour figure can be viewed at wileyonlinelibrary.com]

The injection-shut-in case has been validated using a numerical code, FLAC-TOUGHREACT.[22,27] This code coupled the thermal and hydrologic capabilities of TOUGHREACT with the mechanical framework of FLAC^{3D} to examine THM processes in deformable fractured media. The specific target of this code development was stimulation. For the current example, stimulation effects on the permeability were not considered in FLAC-TOUGH; we here wish to examine the validity of our own code.

Figure 4 presents the pore pressure development. A good agreement is achieved. During shut-in, pressures shortly after the change of rate show a mismatch related to the approximation of fully developed flow for all times, which is not valid immediately after the change of rate; see the discussion in Section 2.2. However, the effect quickly disappears.

Comparisons of calculated radial and tangential stresses are provided in Figure 5. We see indeed a good match of the outcomes of the two codes. The largest effect is seen in the radial stress; the total tangential stresses are virtually constant. This implies, however, that the effect of the pore pressure on the effective tangential stresses is considerable.

Figure 6 presents the comparison of developing criticality, during injection and during shut-in. Indeed, we see a good agreement between the two models. Both models show criticality decreasing at the wellbore after commencing injection, while it perseveres further away; after shut-in, the situation reverses and criticality is seen again close to the wellbore. The mismatch that we see is related to the approximation of the full transient solution with the semisteady-state solution, the approximation of the plasticity radius, and the numerical implementation of pressures and stresses in FLAC-TOUGH. Also, the implementation of the coupling in FLAC-TOUGH may not be completely consistent with our definition of the Biot modulus. This can also be the background for the mismatch in displacements and volumetric strains (Figure 7). We deem the agreement sufficient for validation of our coupled code; we refer to the discussion (Section 4) for some additional remarks.

One of the goals of our approach was to be able to include permeability changes. To this end, we adapted the base case through the introduction of a fracture network with spacing 0.5 m. As a result, the permeability is greatly increased upon the creation of volume strain. The pressure gradient consequently decreases considerably in the affected area, and

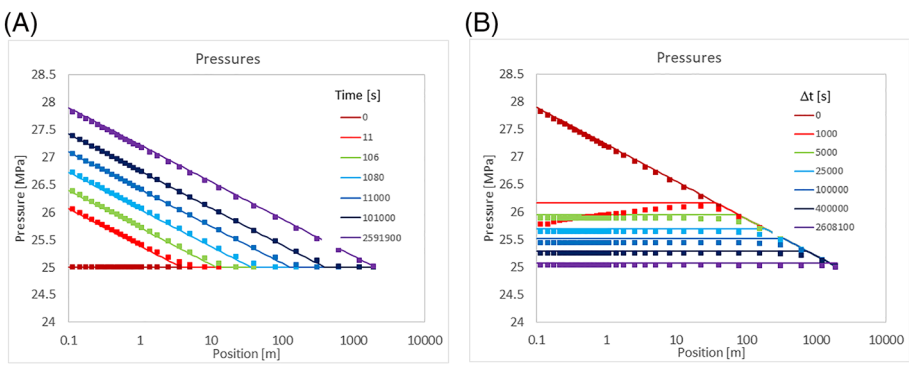

FIGURE 4 Validation of the pressure development for injection-shut-in case with TOUGH-FLAC. Symbols are calculated with TOUGH-FLAC; lines with our code. Left: during injection. Right: during shut-in [Colour figure can be viewed at wileyonlinelibrary.com]

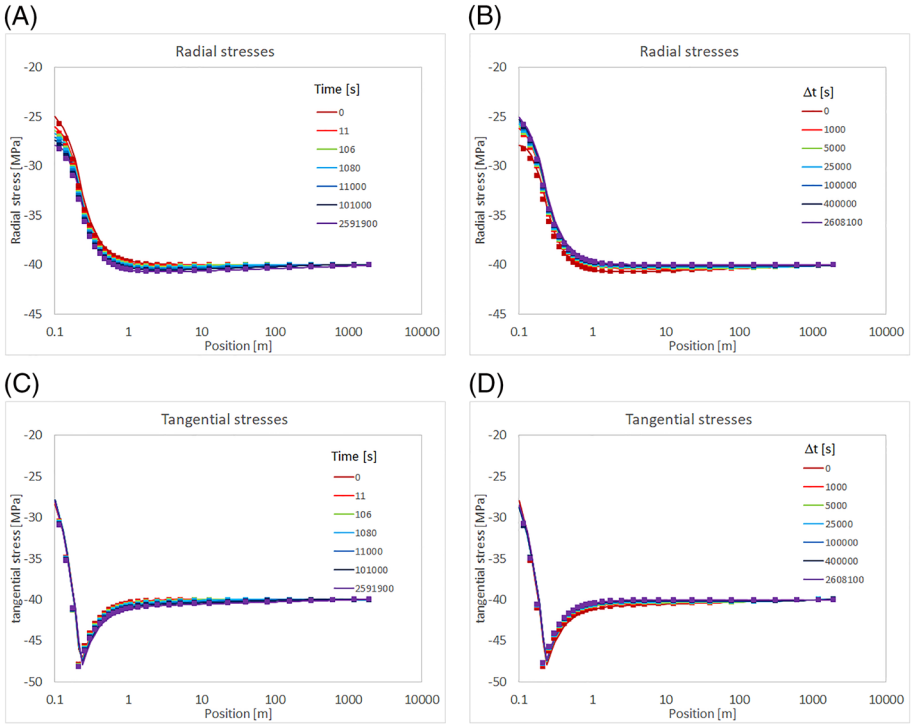

FIGURE 5 Validation of the stresses for the injection-shut-in case with TOUGH-FLAC. Top: radial stresses; Bottom: tangential stresses. Left: during injection; Right: during shut-in [Colour figure can be viewed at wileyonlinelibrary.com]

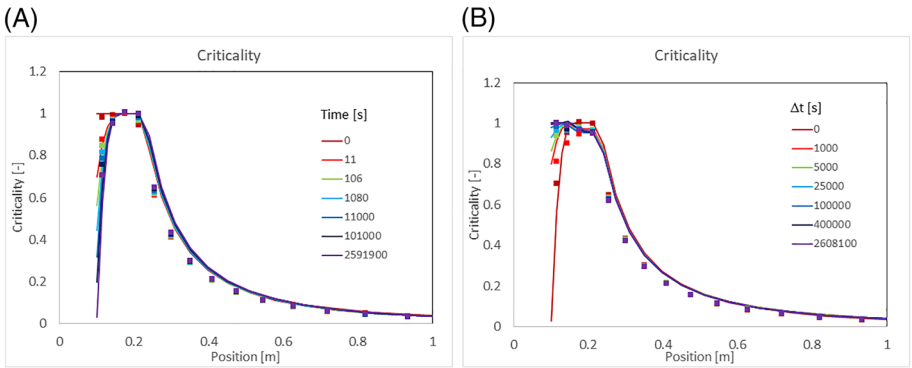

FIGURE 6 Validation of the injection-shut-in case with TOUGH-FLAC: Development of critical behavior during injection (left) and during pressure falloff after shut-in (right) [Colour figure can be viewed at wileyonlinelibrary.com]

the injectivity increases. The effects during the injection period are shown in Figure 8, the effects during the shut-in are shown in Figure 9. The effect on the resulting injectivity for this particular case is in the order of 25%.

A common procedure is to flow back after stimulation. We have performed a simulation with flowback; the results are presented in Figure 10. The curves start again at the end of the stimulation (Figure 8).

As a first observation, we note that the pressure at the wellbore decreases below the original pressure. The effects on the stresses are larger than in the shut-in case as a result of the larger change in rate. Further, the stimulation effect close to the well is maintained, but beyond the original plasticity radius, elastic compression causes a decrease in permeability.

4 | DISCUSSION

In the present section, we discuss a number of issues that have arisen and how to approach them. Some will be addressed in ongoing and planned research; others fall outside the scope of our semianalytic approach and warrant the use of numerical tools.

We have employed a plane strain approach in our model. Vertical stresses are calculated and they contribute to the mechanical response, but they have not been considered as essentially contributing to plasticity. The plane-strain approximation implies that the possible effect of a finite height of the layers in which the pressure disturbances occur is

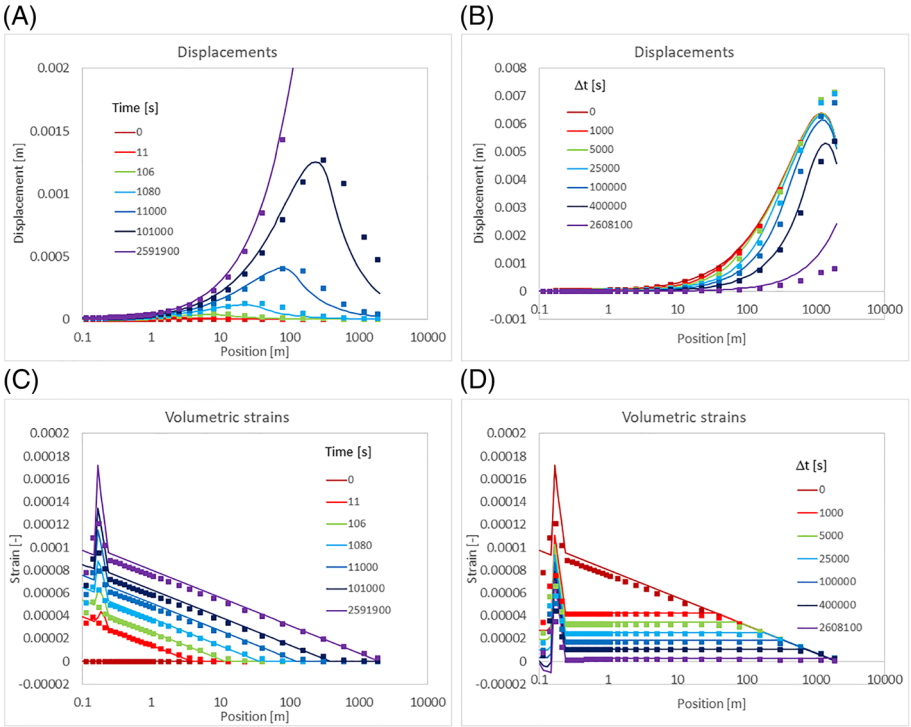

FIGURE 7 Validation of the injection-shut-in case with TOUGH-FLAC: Development of the displacements (top) and volumetric strains (bottom) during injection (left) and during pressure falloff after shut-in (right). Displacements and strains are given with respect to the values at time 0 [Colour figure can be viewed at wileyonlinelibrary.com]

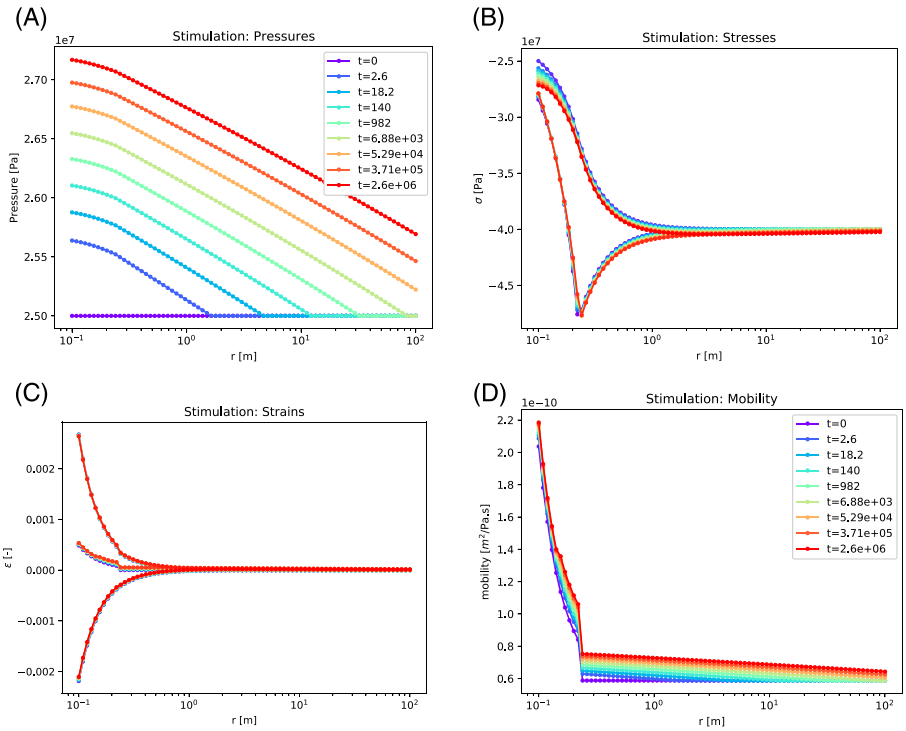

FIGURE 8 Key results of stimulation scenario during injection. Top row: Pressures and stresses. Bottom row: strains (extensional radial strains; compressive tangential strains; combining to extensional volume strains) and the resulting effect on the fluid mobility through the permeability increase [Colour figure can be viewed at wileyonlinelibrary.com]

not incorporated. Different approaches can be envisioned to address these issues. For the incorporation of the vertical stress, the start should be from the elastic response. If the combination of effective vertical and horizontal stress exceeds the failure criterion, plasticity may be employed to reduce the vertical stress. For the effect of a finite height, approaches like the one by[28] could be considered. They could be benchmarked with exact solutions available for cylindrical zones with constant temperature or pressure disturbance.[29-31]

In addition to the plane-strain approximation, we have limited ourselves to a radial symmetry. Any plastic zone is thus bounded by one or two radii of elastic-plastic transition.[16,17] An extension to nonradial symmetries would be very beneficial, in particular for strike-slip faulting regimes. This, however, is a major effort since the equations complicate

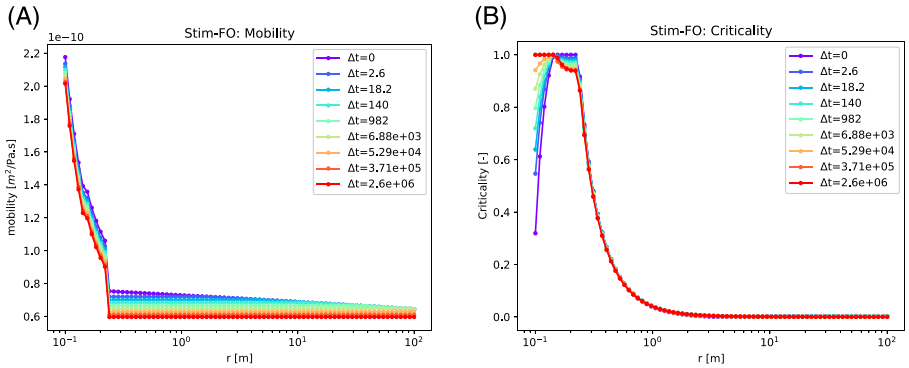

FIGURE 9 Results during shut-in following stimulation. Criticality develops in a similar fashion as the case above; the permeability is not completely reversed to the starting values—this is due to the persistent result of plastic flow [Colour figure can be viewed at wileyonlinelibrary.com]

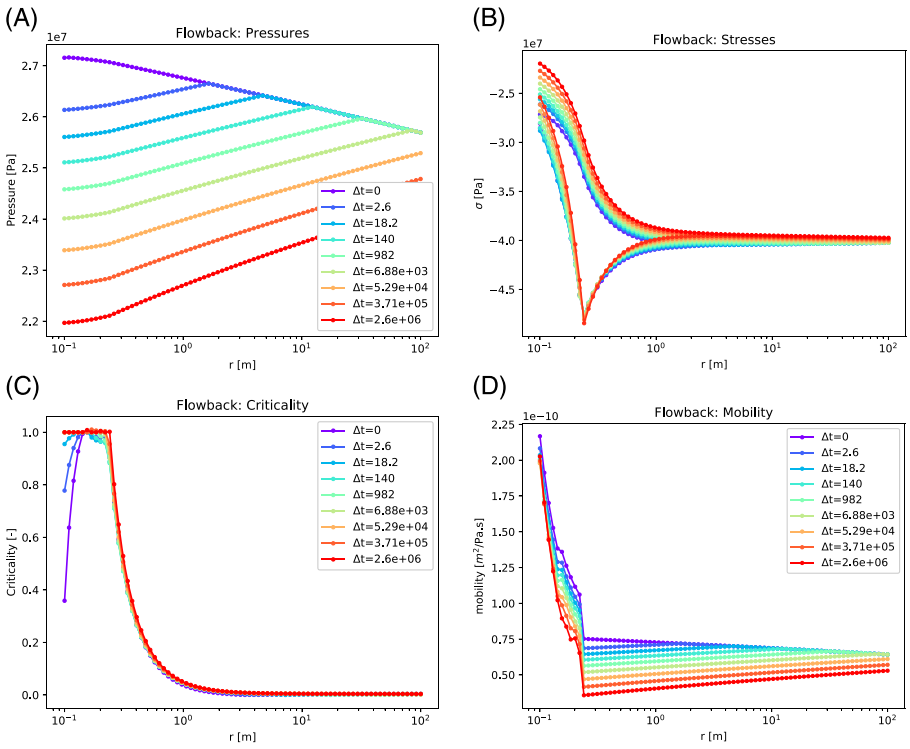

FIGURE 10 Results during flowback stimulation. Criticality develops in a similar fashion as the case above; the permeability is not more than completely reversed to the starting values—this is due to the elastic part of the response of the strain to the stresses [Colour figure can be viewed at wileyonlinelibrary.com]

considerably. A possible approach is in the line of Galin[48] and Detrounay and Fairhurst,[32] who proposed solutions for limited stress ratios with forms of an elliptical yield zone around a circular cavity. However, a numerical approach may still be warranted, in particular when also the plane-strain approximation needs to be abandoned).

Another limitation connected to the radial symmetry is that it limits the application to isotropic flow and mechanical properties in the horizontal directions. Constitutive models are readily available,[33-35] but implementation in the current workflow will be complicated. A simple scaling of axes as is sometimes appropriate for uncoupled flow problems[36] is not appropriate since the flow and the mechanics will scale differently.

The examples we presented showed tangential stresses staying below the pore pressure: no dilatational stresses developed. Larger injection rates, smaller permeabilities or continued injection might result in such dilatational stresses. Then, fluidization might occur close to the wellbore, even with pressures well below the minimum in situ stress. Such situations must be treated with models different from the simple elastic—perfectly plastic models that we employed here. We do not see fundamental difficulties on the way to such implementation.

Thermoelastic stresses can be considered in the same way as poro-elastic stresses,[37] but the heat transfer is different from pressure diffusion. In fact, thermal energy is transported by convection and by conduction—when neglecting radiation. Using either conduction-dominated or convection-dominated transport will often be a suboptimal approximation, but it could be a good first start.

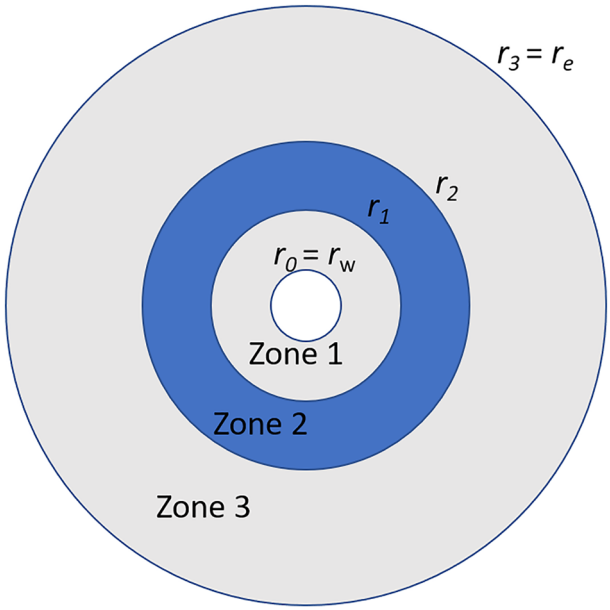

FIGURE 11 Visualization of a three-zone system with associated boundaries and interfaces [Colour figure can be viewed at wileyonlinelibrary.com]

Important effects can happen due to chemical reactions, precipitation, dissolution, and swelling.[38,39] This can be related to the high temperatures and large temperature differences manifest in geothermal applications, and the chemical response of different minerals and solutes present. One can also think about the use of fluids different from water. We feel our setup is promising in the sense that it is flexible enough to also incorporate such phenomena.

The present paper is in the first place a methodology paper. We have therefore focused on the specifics of the method, and we have chosen examples to demonstrate these. We are currently working on applications to field cases, on the implementation of thermoelastic stresses and of more complicated plastic models. Examples of the latter are the Elastic-Brittle-Perfectly plastic model[17,18]; the Modified Cam Clay model,[19,40,41] the hardening-softening model with a Drucker-Prager condition[20,35]; viscoplasticity,[42] and the Mogi-Coulomb failure model that accounts for the intermediate stress.[43,44] As these models are based on laboratory measurements, our fast semianalytic approach will be helpful in investigating the consequences on reservoir scale.

Enhanced Geothermal Systems usually target low-permeability, fractured rock like granites or volcanic rock.[45] For such systems, plasticity models may not be appropriate. Here, fracture network models can be employed. Rutqvist et al[46] give an example of such a model in the numerical domain. What is additionally required within our setup is the implementation of the mechanic response of the fracture network.

5 | CONCLUDING REMARKS

We have devised, implemented, tested, and demonstrated a semianalytic coupled poro-elasto-plastic model for wellbore stability and stimulation. As it fundamentally employs a sequential time-dependent scheme, it is optimally suitable for time-dependent plasticity, for tracking developing reservoir properties, and for operational scenarios with changing injection or production rates. Plastic behaviour can take place close to the wellbore, but also in isolated regions away from it. This depends on the specifics of the driving parameters. Our tool can be easily used in data assimilation workflows and in optimization. Further, it is ideal for assessing the large-scale effects of laboratory-derived models and of their driving parameters. Extensions envisaged for application to geothermal energy include thermal effects and more advanced plasticity models.

ACKNOWLEDGEMENTS

The project leading to the results in this article received funding from the European Union's Horizon 2020 research and innovation programmes under grant agreement nos 691728 and 727550.

ORCID

Peter A. Fokker https://orcid.org/0000-0001-9366-1497

REFERENCES

1. King GE. Thirty years of gas shale fracturing: what have we learned? In: *In SPE Annual Technical Conference and Exhibition*. Society of Petroleum Engineers; 2010, January.
2. Lu SM. A global review of enhanced geothermal system (EGS). *Renewable and Sustainable Energy Reviews*. 2018;81:2902-2921.
3. Lee KK, Ellsworth WL, Giardini D, et al. Managing injection-induced seismic risks. *Science*. 2019;364(6442):730-732.
4. Wassing BBT, Van Wees JD, Fokker PA. Coupled continuum modeling of fracture reactivation and induced seismicity during enhanced geothermal operations. *Geothermics*. 2014;52:153-164.
5. Ghassemi A. A review of some rock mechanics issues in geothermal reservoir development. *Geotechnical and Geological Engineering*. 2012;30(3):647-664.
6. Hofmann H, Zimmermann G, Farkas M, et al. First field application of cyclic soft stimulation at the Pohang Enhanced Geothermal System site in Korea. *Geophysical Journal International*. 2019;217(2):926-949.
7. Jansen JD, Brouwer R, Douma SG. Closed loop reservoir management. In: *In SPE reservoir simulation symposium*. Society of Petroleum Engineers; 2009, January.
8. Evensen G. *Data assimilation: the ensemble Kalman filter*. Springer Science & Business Media; 2009.
9. Gaucher E, Schoenball M, Heidbach O, et al. Induced seismicity in geothermal reservoirs: a review of forecasting approaches. *Renewable and Sustainable Energy Reviews*. 2015;52:1473-1490.
10. Bai M, Abousleiman Y. Thermoporoelastic coupling with application to consolidation. *International Journal for Numerical and analytical methods in Geomechanics*. 1997;21(2):121-132.
11. Rice JR, Cleary MP. Some basic stress diffusion solutions for fluid-saturated elastic porous media with compressible constituents. *Reviews of Geophysics*. 1976;14(2):227-241.
12. Detournay E, Cheng AD. Poroelastic response of a borehole in a non-hydrostatic stress field. *In International Journal of Rock Mechanics and Mining Sciences & Geomechanics Abstracts*. 1988;25(3):171-182. Pergamon
13. Bai M, Roegiers JC. Fluid flow and heat flow in deformable fractured porous media. *International journal of engineering science*. 1994;32 (10):1615-1633.
14. Tao Q, Ghassemi A. Poro-thermoelastic borehole stress analysis for determination of the in situ stress and rock strength. *Geothermics*. 2010;39(3):250-259.
15. Wang Y, Dusseault MB. Borehole yield and hydraulic fracture initiation in poorly consolidated rock strata—part II. Permeable media. *In International journal of rock mechanics and mining sciences & geomechanics abstracts*. 1991;28(4):247-260. Pergamon
16. Han G, Dusseault MB. Description of fluid flow around a wellbore with stress-dependent porosity and permeability. *Journal of petroleum science and engineering*. 2003;40(1-2):1-16.
17. Masoudian MS, Hashemi MA. Analytical solution of a circular opening in an axisymmetric elastic-brittle-plastic swelling rock. *Journal of Natural Gas Science and Engineering*. 2016;35:483-496.
18. Masoudian MS, Hashemi MA, Tasalloti A, Marshall AM. Elastic–brittle–plastic behaviour of shale reservoirs and its implications on fracture permeability variation: An analytical approach. *Rock Mechanics and Rock Engineering*. 2018;1-18.
19. Chen SL, Abousleiman YN. Exact drained solution for cylindrical cavity expansion in modified Cam Clay soil. *Géotechnique*. 2013;63(6): 510-517.
20. Chen SL, Abousleiman YN. Cavity expansion in strain hardening frictional soils under drained condition. *International Journal for Numerical and Analytical Methods in Geomechanics*. 2018;42(1):132-142.
21. Settari A, Walters DA. Advances in coupled geomechanical and reservoir modeling with applications to reservoir compaction. *Spe Journal*. 2001;6(03):334-342.
22. Taron J, Elsworth D. Thermal–hydrologic–mechanical–chemical processes in the evolution of engineered geothermal reservoirs. *International Journal of Rock Mechanics and Mining Sciences*. 2009;46(5):855-864.
23. Dake LP. *Fundamentals of reservoir engineering (Vol. 8)*. Elsevier; 1983.
24. Grant MA, Bixley PF. *Geothermal Reservoir Engineering*. Academic Press; 2011.
25. Jaeger JC, Cook NG, Zimmerman R. *Fundamentals of rock mechanics*. John Wiley & Sons; 2007.
26. Bai M, Elsworth D. Modeling of subsidence and stress-dependent hydraulic conductivity for intact and fractured porous media. *Rock mechanics and rock engineering*. 1994;27(4):209-234.
27. Fokker PA, Wassing BBT. A fast model for THM processes in geothermal applications. In: *Presented at the European Geothermal Congress, 11 – 14 June 2019*. The Hague: The Netherlands; 2019.
28. Atefi Monfared K, Rothenburg L. Poro-elasto-plastic response of an unconsolidated formation confined with stiff seal rocks under radial injection. *International Journal for Numerical and Analytical Methods in Geomechanics*. 2016;40(13):1799-1826.
29. Candela T, van der Veer EF, Fokker PA. On the importance of thermo-elastic stressing in injection-induced earthquakes. *Rock Mechanics and Rock Engineering*. 2018;51(12):3925-3936.
30. Myklestad NO. Two problems of thermal stress in the infinite solid. *J Appl Mech*. 1942;9:136-143.
31. Perkins TK, Gonzalez JA. The effect of thermoelastic stresses on injection well fracturing. *Society of Petroleum Engineers Journal*. 1985; 25(01):78-88.
32. Detournay E, Fairhurst C. Two-dimensional elastoplastic analysis of a long, cylindrical cavity under non-hydrostatic loading. *In International Journal of Rock Mechanics and Mining Sciences & Geomechanics Abstracts*. 1987;24(4):197-211. Pergamon

33. Semnani SJ, White JA, Borja RI. Thermoplasticity and strain localization in transversely isotropic materials based on anisotropic critical state plasticity. *International Journal for Numerical and Analytical Methods in Geomechanics*. 2016;40(18):2423-2449.
34. Zhang Q, Choo J, Borja RI. On the preferential flow patterns induced by transverse isotropy and non-Darcy flow in double porosity media. *Computer Methods in Applied Mechanics and Engineering*. 2019;353:570-592.
35. Zhao Y, Semnani SJ, Yin Q, Borja RI. On the strength of transversely isotropic rocks. *International Journal for Numerical and Analytical Methods in Geomechanics*. 2018;42(16):1917-1934.
36. Bear J. *Hydraulics of groundwater New York*. Mc GrawHill Inc.; 1979.
37. Perkins TK, Gonzalez JA. Changes in earth stresses around a wellbore caused by radially symmetrical pressure and temperature gradients. *Society of Petroleum Engineers Journal*. 1984;24(02):129-140.
38. Liu J, Fokker PA, Spiers CJ. Coupling of swelling, internal stress evolution, and diffusion in coal matrix material during exposure to methane. *Journal of Geophysical Research: Solid Earth*. 2017;122(2):844-865.
39. Tao J, Wu Y, Elsworth D, Li P, Hao Y. Coupled thermo-hydro-mechanical-chemical modeling of permeability evolution in a CO_2-circulated geothermal reservoir. *Geofluids*. 2019;2019:1-15.
40. Davis RO, Selvadurai AP. *Plasticity and geomechanics*. Cambridge university press; 2005.
41. Pijnenburg RPJ, Verberne BA, Hangx SJT, Spiers CJ. Inelastic deformation of the Slochteren sandstone: stress-strain relations and implications for induced seismicity in the Groningen gas field. *Journal of Geophysical Research: Solid Earth*. 2019;124. https://doi.org/10.1029/2019JB017366
42. Borja RI, Yin Q, Zhao Y. Cam-Clay plasticity. Part IX: On the anisotropy, heterogeneity, and viscoplasticity of shale. *Computer Methods in Applied Mechanics and Engineering*. 2019;1-25.
43. Al-Ajmi AM, Zimmerman RW. Relation between the Mogi and the Coulomb failure criteria. *International Journal of Rock Mechanics and Mining Sciences*. 2005;42(3):431-439.
44. Singh A, Rao KS, Ayothiraman R. An analytical solution for a circular wellbore using Mogi-Coulomb failure criterion. *Journal of Rock Mechanics and Geotechnical Engineering. (Accepted).* 2019.
45. Olasolo P, Juárez MC, Morales MP, Liarte IA. Enhanced geothermal systems (EGS): a review. *Renewable and Sustainable Energy Reviews*. 2016;56:133-144.
46. Rutqvist J, Leung C, Hoch A, Wang Y, Wang Z. Linked multicontinuum and crack tensor approach for modeling of coupled geomechanics, fluid flow and transport in fractured rock. *Journal of Rock Mechanics and Geotechnical Engineering*. 2013;5(1):18-31.
47. Fjaer E, Holt RM, Raaen AM, Risnes R, Horsrud P. *Petroleum related rock mechanics (Vol. 53)*. Elsevier; 2008.
48. Galin LA. *Plane elastic-plastic problem: plastic regions around circular holes in plates and beams*. Division of Applied Mathematics: Brown University; 1947.

How to cite this article: Fokker PA, Singh A, Wassing BBT. A semianalytic time-resolved poro-elasto-plastic model for wellbore stability and stimulation. *Int J Numer Anal Methods Geomech*. 2020;44:1032–1052. https://doi.org/10.1002/nag.3048

APPENDIX A.

A.1. | Geometry and equations for a three-zone system

To help the reader visualize the division in concentric domains and the associated equations for the boundary and interface conditions, we here represent the geometry and the equations for a three-zone system. Figure 11 indicates the zones in the domain: the wellbore in the middle; then an elastic zone (l=0) in grey, a plastic zone (l=1) in blue, and another elastic zone (l=2) towards infinity. The influence radius $r_3 = r_e$ is also indicated, but it does not limit the elastic boundary. Only the pressure disturbance does not reach further.

The inner elastic zone has parameters $Z_{1,1}$ and $Z_{2,1}$; the plastic zone has parameters $\sigma^A_{rr,2}$ and $\delta u_{A,2}$; the outer elastic zone has parameters $Z_{1,3}$ and $Z_{2,3}$.

The equations for the boundaries of these zones read:

Radial stress in the inner elastic zone equals the pressure in the wellbore:

$$\frac{Z_{1,1}}{r_w^2} - \frac{Z_{2,1}}{2(1-2\nu)} = \sigma^i_{rr}(r_w) + P_w.$$

Continuity of radial stresses: at the interface of elastic zone 1 to plastic zone 2

$$\sigma_{rr}^{i}(r_1)-\frac{1}{r_1^2}\left[\Delta I_{PT}^{i+1}(r_1,t)+Z_{1,1}\right]+\frac{Z_{2,1}}{2(1-2\nu)}=\sigma_{rr,2}^{A}.$$

Continuity of displacements at the interface of elastic zone 1 to plastic zone 2

$$\delta u_{A,2}=\frac{1}{r_1\cdot 2G}\left\{\Delta I_{PT}^{i+1}(r_1)+Z_{1,1}+\frac{1}{2}Z_{2,1}r_1^2\right\}.$$

Continuity of radial stresses at the interface of plastic zone 2 to elastic zone 3

$$\frac{r_2^{\gamma-1}}{r_1^{\gamma-1}}\sigma_{rr,2}^{A}+r_2^{\gamma-1}\left[\frac{P(r_l)}{r_1^{\gamma-1}}-\int_{r_1}^{r_2}g(\gamma)\frac{d\rho}{\rho^{\gamma}}\right]-P(r_2)=\sigma_{rr}^{i}(r_2)-\frac{1}{r_2^2}\left[\Delta I_{PT}^{i+1}(r_2,t)+Z_{1,3}\right]+\frac{Z_{2,3}}{2(1-2\nu)}.$$

Continuity of displacements at the interface of plastic zone 2 to elastic zone 3

$$\delta u_{A,2}\left(\frac{r_2}{r_1}\right)^{-\beta}+\sigma_{rr,2}^{A}r_2^{-\beta}\int_{r_1}^{r_2}\rho^{\beta}f_1(\rho)d\rho+r_2^{-\beta}\int_{r_1}^{r_2}\rho^{\beta}f_2(\rho)d\rho=\frac{1}{r_2\cdot 2G}\left\{\Delta I_{PT}^{i+1}(r_2)+Z_{1,3}+\frac{1}{2}Z_{2,3}r_2^2\right\}.$$

No displacement at infinity (1 equation)

$$Z_{2,3}=0.$$

Together, these equations form a linear set in the parameters $Z_{1,1}$; $Z_{2,1}$; $\sigma_{rr,2}^{A}$; $\delta u_{A,2}$; $Z_{1,3}$; and $Z_{2,3}$:

$$\begin{pmatrix} \frac{1}{r_w^2} & \frac{-1}{2(1-2\nu)} & 0 & 0 & 0 & 0 \\ \frac{1}{r_1^2} & \frac{-1}{2(1-2\nu)} & 1 & 0 & 0 & 0 \\ \frac{-1}{r_1\cdot 2G} & \frac{-r_1}{4G} & 0 & 1 & 0 & 0 \\ 0 & 0 & \frac{r_2^{\gamma-1}}{r_1^{\gamma-1}} & 0 & \frac{1}{r_2^2} & \frac{-1}{2(1-2\nu)} \\ 0 & 0 & r_2^{-\beta}\int_{r_1}^{r_2}\rho^{\beta}f_1(\rho)d\rho & \left(\frac{r_2}{r_1}\right)^{-\beta} & \frac{-1}{r_2\cdot 2G} & \frac{-r_2}{4G} \\ 0 & 0 & 0 & 0 & 0 & 1 \end{pmatrix}\begin{pmatrix} Z_{1,1} \\ Z_{2,1} \\ \sigma_{rr,2}^{A} \\ \delta u_{A,2} \\ Z_{1,3} \\ Z_{2,3} \end{pmatrix}$$

$$=\begin{pmatrix} \sigma_{rr}^{i}(r_w)+P_w \\ \sigma_{rr}^{i}(r_1)-\frac{1}{r_1^2}\Delta I_{PT}^{i+1}(r_1,t) \\ \frac{\Delta I_{PT}^{i+1}(r_1)}{r_1\cdot 2G} \\ P(r_2)+\sigma_{rr}^{i}(r_2)-\frac{\Delta I_{PT}^{i+1}(r_2,t)}{r_2^2}-r_2^{\gamma-1}\left[\frac{P(r_l)}{r_1^{\gamma-1}}-\int_{r_1}^{r_2}g(\gamma)\frac{d\rho}{\rho^{\gamma}}\right] \\ -r_2^{-\beta}\int_{r_1}^{r_2}\rho^{\beta}f_2(\rho)d\rho+\frac{\Delta I_{PT}^{i+1}(r_2)}{r_2\cdot 2G} \\ 0 \end{pmatrix}.$$